hydrology

Article

Multi-Scale Analysis of Meteorological and Hydrological Droughts in the Yujiang River Basin of Southern China: Response Mechanisms and Influencing Factors

Yanbing Huang, Xiaoli Yang *, Xungui Li *, Jian Sun, Qiyong Yang, Xu Dong and Yongjun Huang

College of Civil Engineering and Architecture, Guangxi University, 100 East Daxue Road, Nanning 530004, China; 2310303004@st.gxu.edu.cn (Y.H.); 2210403003@st.gxu.edu.cn (J.S.); 2310403007@st.gxu.edu.cn (Q.Y.); 2310303002@st.gxu.edu.cn (X.D.); gxslhyj@st.gxu.edu.cn (Y.H.)

* Correspondence: 2210303017@st.gxu.edu.cn (X.Y.); xunguili@gxu.edu.cn (X.L.)

Abstract

Drought exhibits a complex coupling response to regional meteorological factors, hydrological characteristics, land cover, and large-scale teleconnection climate indices, while their direct and indirect influences on multi-scale meteorological and hydrological droughts remain insufficiently understood, particularly in karst basins. This study investigated drought dynamics in China's Yujiang River Basin using an integrated framework combining run theory, drought propagation analysis, and the partial least squares–structural equation model (PLS-SEM). We analyzed the 1-, 3-, 6-, and 12-month standardized precipitation index (SPI) and standardized streamflow index (SSI) at four hydrological stations during 1984–2014, together with meteorological factors, land cover indices, large-scale climate indices, areal precipitation, and naturalized streamflow. The results show that precipitation and streamflow exhibited slight declining tendencies with marked seasonal variability, and that drought durations of all severity levels generally decreased with increasing time scales. At the same time scale, SSI was more stable than SPI, and both indices tended to become more stable as the time scale increased. SPI-3 and SSI-1 were identified as the optimal time scales for monitoring meteorological and hydrological drought, respectively, providing a practical basis for drought identification and early warning in karst basins. Hydrological drought lagged meteorological drought by 1–3 months, indicating a measurable propagation time that is valuable for improving drought preparedness and water resources regulation. PLS-SEM further revealed that precipitation and streamflow were the dominant direct drivers of drought development, while land cover exerted a persistent negative effect, and climate-related factors mainly influenced drought indirectly. These findings enhance the understanding of drought propagation and multi-factor coupling mechanisms in karst basins and provide scientific support for regional drought monitoring and water resources management.

Keywords: meteorological drought; hydrological drought; multi-scale response mechanism; lag response time; influencing factors; Yujiang River Basin

Academic Editor: Luca Brocca

Received: 30 March 2026
Revised: 26 April 2026
Accepted: 6 May 2026
Published: 13 May 2026

1. Introduction

Drought is one of the most complex and widespread natural disasters globally [1], with global warming exacerbating the complexity and randomness of extreme meteorological and hydrological events. Meteorological drought is defined as a period of insufficient precipitation, while hydrological drought is reflected through the depletion of streamflow or reservoir levels [2,3]. The standardized precipitation index (SPI) and the standardized streamflow index (SSI) are ideal choices for distinguishing between meteorological and hydrological drought types [4,5]. These two drought indices can reflect different stages of drought to some extent [6]. Drought assessment is based on various drought indicators, and different time scales can also affect drought evaluation [7], leading to uncertainty in the results. Generally, meteorological drought develops and ends more rapidly, while hydrological drought lags behind the occurrence of meteorological drought [8]. The propagation time depends on local landscape characteristics; therefore, although the occurrence mechanisms and evolution patterns of meteorological and hydrological drought differ, there is a lagged connection and complex response relationship between the two [6].

The intensification of global warming poses significant challenges for the monitoring and prediction of drought events within watersheds [9], and the issue of drought is expected to become even more severe in the future [3]. Drought events are typically triggered by extreme changes in natural climate conditions, leading to drastic fluctuations in regional meteorological factors [5], which further affect land cover and the regional ecological environment, altering hydrological characteristics and drought information [10]. Studies have indicated that during the evolution of drought events, there is a close relationship between drought and large-scale climate indices (e.g., atmospheric-oceanic circulation indices), small-scale meteorological factors (e.g., air temperature, pressure, etc.), regional precipitation, streamflow, and changes in land cover (e.g., vegetation cover, leaf area index) [11–13]. Therefore, when assessing the impact of different factors on drought, it is essential to quantify both the direct effects of multiple factors on drought and to consider their indirect effects. Thus, conducting research on the influencing factors of hydrometeorological drought and revealing their direct and indirect impact mechanisms is exceptionally important.

Traditional empirical statistics and regional hydrological models struggle to accurately quantify the direct and indirect complex relationships between latent variables such as large-scale climate, regional meteorological and hydrological characteristics, vegetation dynamics, and drought. These variables are often treated as independent of one another, but this assumption deviates significantly from reality. Moreover, most studies are limited to drought indices of the same type at different scales or different types at the same scale, with few exploring the comprehensive impacts of climate, meteorological, hydrological characteristics, and vegetation dynamics on various types and scales of drought simultaneously.

In recent years, the structural equation model (SEM) has been widely used to study the relationships between independent and dependent variables, particularly demonstrating unique advantages in research on different influence paths (direct and indirect effects) [14,15]. Compared with traditional statistical analysis methods, the partial least squares-SEM (PLS-SEM) can quantitatively explore the effect of individual indicators on the overall outcome and the interrelationships among individual indicators through methods such as multiple regression, principal component analysis, path analysis, factor analysis, and covariance analysis [16–19]. It enables an in-depth analysis of the complex response mechanisms of multi-scale meteorological and hydrological droughts to multiple potential variables (such as large-scale teleconnection climate indices, regional meteorological factors, areal precipitation, naturalized streamflow, and dynamics of land cover) and is a useful method worth exploring.

Since 1961, the frequency of drought events in Southern China has been increasing year by year, with both intensity and frequency continuing to rise [20]. This poses a serious threat to agricultural production and ecosystems, resulting in significant losses for residents in terms of both livelihood and property. The Yujiang River Basin (YRB), located in Southern China, is one of the largest contiguous karst regions in the world. Its unique karst geographical environment significantly impacts the process of precipitation transforming

https://doi.org/10.3390/hydrology13050131

into streamflow, increasing the complexity of drought causes in the region and making ecosystems more vulnerable during drought events [21]. Therefore, the goals in this study are: (i) to develop a PLS-SEM framework to investigate the complex response relationships among multi-source influencing factors and multi-scale meteorological and hydrological droughts, by linking observable variables to key latent processes including climate forcing, meteorological conditions, land cover, precipitation, and streamflow (ii) to further quantify the complex dependent causal relationships between meteorological and hydrological droughts in the YRB across different time scales and confirms the varying impacts of different types of factors on hydrological and meteorological droughts. The main innovations and academic contributions of this study are reflected in the following three aspects: (i) This study establishes a multi-scale, multi-variable, and multi-type drought analysis framework, enabling the integrated investigation of meteorological and hydrological droughts and their interactions under multiple driving factors. This approach moves beyond the traditional assumption of independent variables and provides a more realistic representation of multi-factor coupling mechanisms. (ii) This study integrates run theory, drought propagation analysis, and PLS-SEM into a unified framework to systematically quantify the multi-factor coupling mechanisms and scale-dependent responses of meteorological and hydrological droughts. (iii) The unique karst environment in the YRB significantly affects the process of precipitation converting to streamflow, increasing the complexity of drought causes in the region. This paper summarizes the characteristics of drought variation and the temporal and spatial distribution patterns in the YRB, providing a theoretical basis for reducing regional drought risk. The findings can serve as a reference for the scientific management of water resources in the YRB.

2. Materials and Methods

2.1. Study Area

The YRB (21°31′–24°38′ N, 104°30′–110°16′ E) is the largest component of the Xijiang River system in the Pearl River Basin of Southern China, featuring typical karst landforms. The basin covers an area of 89,691.5 km^2, with the main river stretching 1152 km in length. The terrain gradually descends from the northwest to the southeast, with an average gradient of 0.314‰. The main river exhibits a medium-sized mountainous canyon topography above the Baise Hydrological Station (Figure 1), while below the station, hilly areas and vast basins are interspersed. The tributary of Pearl River is mostly karst erosion plains; the area below Nanning Station is characterized by hilly plains.

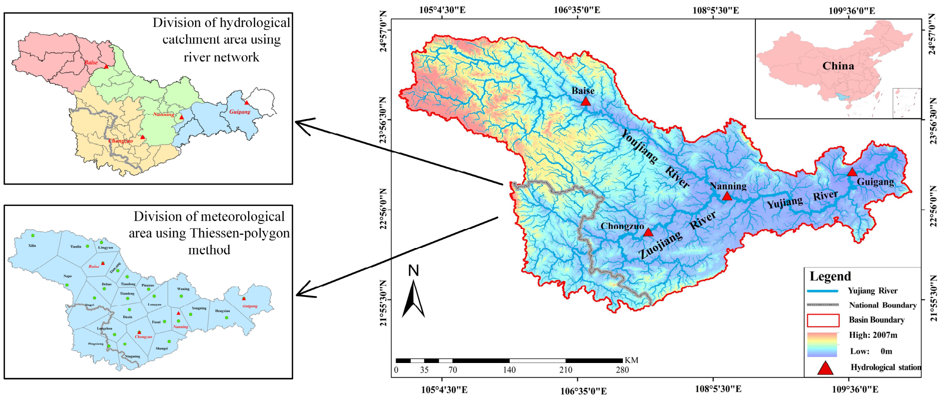

Figure 1. Locations of study area and hydrological and meteorological stations in the Yujiang River Basin.

The average annual air temperature in the YRB is 17 to 23 °C [22], with an average annual evaporation of 1693 mm [23]. The average relative humidity ranges from 71% to 80%, and the annual average sunshine duration is between 1282 and 2243 h [24], indicating a typical continental monsoon climate and maritime climate. Precipitation is influenced by marine warm air masses and inland air masses, with an average annual precipitation of 1080 to 2760 mm [25], primarily concentrated from June to September, during which heavy rains often occur, mainly caused by typhoons and tropical depressions. The annual average naturalized streamflow (Guigang Station) over 1984–2014 is 44.9 billion m^3, with minimum and maximum values occurring in February and October, respectively. The YRB features diverse vegetation ecosystems, including forests, grasslands, hills, and wetlands [21]. The evolution of meteorological and hydrological factors directly affects vegetation growth, and the dynamic changes in surface coverage exhibit a certain level of resilience to drought disturbances.

The four hydrological stations on the YRB (Baise, Chongzuo, Nanning, and Guigang Stations) are located in the upper left, upper right, midstream, and downstream areas of the basin, respectively (as shown in Figure 1), making them highly representative. Each hydrological station's controlled watershed exhibits unique characteristics in terms of hydrological features, climatic conditions, and biodiversity (land cover). Therefore, this study focuses on the controlled watersheds of these four hydrological stations, combined with data from 24 regional meteorological stations (Figure 1), to reveal the response mechanisms of regional hydrology and meteorological drought, which holds significant practical value.

2.2. Data

This study collected precipitation, streamflow, teleconnection climate factors (sunspot, Ocean Niño, Arctic Oscillation, and North Atlantic Oscillation), meteorological factors (air temperature, evapotranspiration, sunshine duration, relative humidity, and atmospheric pressure), and land cover indices (photosynthetic vegetation fractional cover and leaf area index) from 24 meteorological stations and four typical hydrological stations (Baise, Nanning, Chongzuo, and Guigang) in the YRB over a span of 30 years from 1984 to 2014. Data of daily naturalized streamflow (m^3/s) were provided by the Hydrological Information Center of the Pearl River Water Resources Commission, Ministry of Water Resources of the People's Republic of China. The daily naturalized streamflow data used in this study were obtained from the Hydrological Information Center of the Pearl River Water Resources Commission, Ministry of Water Resources of China. These data were reconstructed using the itemized summation method, which is a standardized approach widely adopted in China for restoring naturalized streamflow in basins affected by human activities. Considering the karst geological characteristics and intensive agricultural activities in the Yujiang River Basin, the reconstruction process conducted by the authority has incorporated multiple correction components, including groundwater variation adjustments, estimation of potential subsurface water exchange, lagged effects of irrigation return flow, and channel transmission losses. These procedures aim to improve the representation of streamflow under near-natural conditions. In principle, the itemized summation method restores naturalized streamflow by correcting the observed streamflow for the effects of major human activities, such as water withdrawal, reservoir regulation, and inter-basin water transfer. Compared with observed streamflow, the reconstructed naturalized streamflow generally exhibits reduced influence from human regulation and better reflects the natural variability of runoff driven by climatic factors. In this study, the naturalized streamflow data from the four hydrological stations (Baise, Chongzuo, Nanning, and Guigang) were directly used without any additional modification or recalibration, ensuring data consistency and reproducibility of the analysis [26]. Daily station precipitation (mm), air temperature (°C), sunshine duration (hours), relative humidity (%), and atmospheric pressure (hPa) of each meteorological station were provided by the China Meteorological Administration https://data.cma.cn/ (accessed on 10 May 2024). The areal precipitation for each hydrological station was calculated within its corresponding upstream controlled catchment rather than over the entire basin. Specifically, the precipitation associated with Baise and Chongzuo stations was aggregated over their respective controlled sub-basins, while the areal precipitation for Nanning and Guigang stations was derived from all relevant upstream meteorological stations within their corresponding controlled catchments. The Thiessen polygon method was used to assign area weights to station precipitation and to estimate catchment-averaged precipitation for each controlled basin. In this way, the precipitation input used in this study is spatially consistent with the hydrological response represented by streamflow at each hydrological station (Figure 1). Evapotranspiration (mm) and photosynthetic vegetation fractional cover (%) data were provided by the Institute of Geographic Sciences and Natural Resources Research, Chinese Academy of Sciences (www.geodata.cn (accessed on 1 May 2024)), while daily leaf area index data were provided by the National Earth System Science Data Center (www.glass.umd.edu (accessed on 5 May 2024)). The daily sunspot index was provided by the Royal Observatory of Belgium (www.astro.oma.be (accessed on 12 May 2024)), and the Ocean Niño index was published as daily data by the National Oceanic and Atmospheric Administration (www.noaa.gov (accessed on 5 May 2024)). The Arctic Oscillation and North Atlantic Oscillation data were provided as monthly data by the National Climate Center (www.ncc-cma.net (accessed on 1 Jule 2024)). All detailed information on the datasets is provided in Table 1. Before PLS-SEM analysis, all variables were unified to a monthly time scale. Daily variables were aggregated to monthly series according to their physical meaning: precipitation and streamflow were converted to monthly totals, whereas air temperature, evapotranspiration, sunshine duration, relative humidity, and atmospheric pressure were converted to monthly averages. The sunspot index, Ocean Niño index, photosynthetic vegetation fractional cover, and leaf area index were also transformed into monthly series, while the Arctic Oscillation and North Atlantic Oscillation were originally available at the monthly scale and were used directly. After temporal aggregation, all variables were aligned over the same study period and standardized before model analysis to ensure consistency and comparability among variables.

Table 1. Data used in this study, data sources, and relevant characteristics.

Data	Data Source	Attribute
Sunspot	Royal Observatory of Belgium (www.astro.oma.be (accessed on 12 May 2024))	Daily
Ocean Niño	National Oceanic and Atmospheric Administration (www.noaa.gov (accessed on 5 May 2024))	
Arctic Oscillation, North Atlantic Oscillation	National Climate Center (www.ncc-cma.net (accessed on 1 Jule 2024))	Monthly
Air temperature Precipitation Sunshine duration Relative humidity Atmospheric pressure	China Meteorological Administration (https://data.cma.cn/ (accessed on 10 May 2024))	Daily
Evapotranspiration	Institute of Geographic Sciences and Natural Resources Research, Chinese Academy of Sciences (www.geodata.cn (accessed on 1 May 2024))	Daily
Photosynthetic vegetation fractional cover		Daily
Leaf area index	National Earth System Science Data Center (www.glass.umd.edu (accessed on 5 May 2024))	Daily
Streamflow	Hydrological Information Center of the Pearl River Water Resources Commission	Daily

2.3. Calculation of SPI and SSI

The value of SPI (*SPI*) is commonly used to monitor drought conditions and quantitatively represents the degree of precipitation deficiency over different periods. It is a meteorological drought calculation index recommended by the World Meteorological Organization. The value of SSI (SSI) essentially reflects the distribution frequency of changes in water deficit. The calculations of the SPI and SSI drought indices are similar [27,28].

When the precipitation (or streamflow) "x" during a certain time period follows a Gamma distribution (Γ), its probability density function $f(x)$ is given by:

$$f(x) = \frac{\beta^{\alpha}}{\Gamma(\alpha)} x^{\alpha-1} e^{-\beta x} \tag{1}$$

where x represents the precipitation or streamflow during a specific time period; α and β are the shape and scale parameters, respectively, and x, α, and β are all greater than 0. The parameters α and β can be calculated using the maximum likelihood method as shown in Equations (2)–(4) [29]:

$$A = ln(\overline{x}) - \sum_{i=1}^{n} \frac{ln(x_i)}{n} \tag{2}$$

$$\beta = \left(1 + \sqrt{1 + 4A/3}\right)/(4A) \tag{3}$$

$$\alpha = \frac{\overline{x}}{\beta} \tag{4}$$

where x_i represents the i-th sample data of precipitation (or streamflow); $\overline{x}$ is the mean for a specific time period; n is the length of the series, or the total number of samples; A is an intermediate variable that simplifies the related calculations for parameter β.

The cumulative probability $F(x)$ of precipitation (or streamflow) x over a certain time scale is given by:

$$F(x) = \int_0^x f(x)x \tag{5}$$

The calculation formula for SPI or SSI obtained through normal standardization of $F(x)$ is:

$$SPI \text{ or } SSI = S\frac{t - (c_2 t + c_1)t + c_0}{((d_3 t + d_2)t + d_1)t + 1.0} \tag{6}$$

$$t = \sqrt{-2ln(F)} \tag{7}$$

where F represents the cumulative probability of precipitation or streamflow over a certain period; S is a constant, usually related to the normal standardization process; t is the transformed value of the cumulative probability $F(x)$; when $F \leq 0.5$, $S = -1$; when $F > 0.5$, $S = 1$; $c_0 = 2.515517$, $c_1 = 0.802853$, $c_2 = 0.010328$, $d_1 = 1.432788$, $d_2 = 0.189269$, $d_3 = 0.001308$ are all empirical values [30].

The classification of drought levels for both SPI and SSI drought indices also shows similarities. When SPI or $SSI \in [-1.0, -0.5)$, it is classified as mild drought; when SPI or $SSI \in [-1.5, -1.0)$, it is classified as moderate drought; when SPI or $SSI \in [-2.0, -1.5)$, it is classified as severe drought; when SPI or $SSI \in [-2.0, -\infty)$, it is classified as extreme drought [31]. For convenience of explanation, this study adopts notations such as SPI-i or SSI-i to represent the SPI or SSI at a time scale of i month(s), where SPI-1 indicates the SPI at a time scale of 1 month.

2.4. Run Theory

The run theory is a time series analysis method that can extract occurrences of the same type of event over time. Let the time series R_t ($t = 1, 2, 3, \ldots, i, \ldots, N$) be truncated at a given level R_x. A negative run occurs when R_t is continuously less than or equal to R_x for a period of time; a positive run occurs when R_t is continuously greater than R_x for a period of time. Based on this, the run intensity and run strength for each segment are obtained as follows:

$$S_t = \sum_{t=i}^{N} R_t, \ \ R_t < R_x \tag{8}$$

$$I_t = \frac{\sum_{t=i}^{N} R_t}{\sum_{t=i}^{N} T_t}, \ R_t < R_x \tag{9}$$

where S_t is the run intensity; I_t is the run strength; T_t is the run length, which indicates the duration from the start to the end of a particular run; R_t is the time series.

This study selects four critical points (R_x) of the SPI and SSI drought indices, namely -0.50, -1.00, -1.50, and -2.00 [32], as the four truncation levels R_0, R_1, R_2, and R_3. It focuses on identifying the number of drought events, duration, intensity, and strength of drought characteristics where the multi-scale meteorological and hydrological drought index series R_t is less than or equal to the four truncation levels R_x, and drought events must last for two months or more, during the period from 1984 to 2014, a total of 30 years. Figure 2 illustrates the process of identifying the run theory of the SPI at the three-month (denoted as SPI-3) series at Chongzuo Station over a 36-month period (from January 2009 to January 2012).

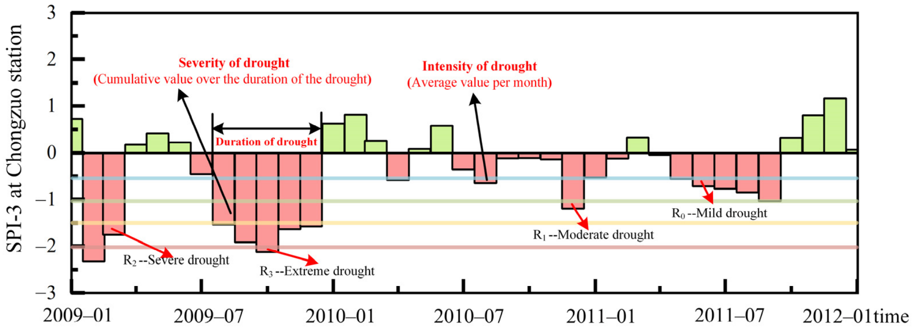

Figure 2. An example illustration of identifying drought process using the run theory for the *SPI*-3 at Chongzuo Station over a 36-month period (from January 2009 to January 2012).

2.5. Partial Least Squares–Structural Equation Model (PLS-SEM)

This study employs PLS-SEM to investigate the causal relationships between different latent variables. The SEM model is divided into a structural model, as shown in Equation (10), and a measurement model, as shown in Equation (11). The structural model addresses the complex relationships among latent variables, while the measurement model considers the relationship between each latent variable and its corresponding observable variables [14]. The PLS-SEM model solves for the components of the measurement model and then estimates the relevant path coefficients in the structural model [33]. Manifest variables are directly observed variables used to construct latent variables, whereas latent variables are those not directly observed in the model but inferred through multiple manifest variables.

Since the naturalized streamflow is determined by calculating measured streamflow using the method of itemized summation commonly widely adopted in China [26]. The value of naturalized streamflow is a calculated value. Therefore, the naturalized streamflow is considered a latent variable. The area-averaged precipitation of the watershed is also derived from the Thiessen polygon method applied to the point precipitation data from various meteorological stations, and this areal precipitation is likewise regarded as a latent variable. Consequently, this study considers seven types of latent variables (large-scale teleconnection climate indices, meteorological factors, land cover, areal precipitation, naturalized streamflow, meteorological drought, and hydrological drought). The observable variables for large-scale teleconnection climate indices include sunspots, Ocean Niño, Arctic Oscillation, and North Atlantic Oscillation. The meteorological factors include air temperature, evapotranspiration, sunshine duration, relative humidity, and atmospheric pressure. The land cover is represented by photosynthetic vegetation fractional cover and leaf area index. The distributional changes in meteorological and hydrological droughts are represented by the *SPI* and *SSI* indices, respectively. The measured streamflow and the measured point precipitation from meteorological stations are no longer included as manifest variables, meaning that the manifest variables considered in this study total eleven: sunspot, Ocean Niño, Arctic Oscillation, North Atlantic Oscillation, air temperature, evapotranspiration, sunshine duration, relative humidity, atmospheric pressure, photosynthetic vegetation fractional cover, and leaf area index.

Structural model (indirect effects between variables):

$$\xi_j = \sum_{i=1}^{i} \beta_{ji}\xi_i + \zeta_j \tag{10}$$

where ξ_j represents the endogenous latent variable (a latent variable influenced by other variables in the model); ξ_i denotes the exogenous latent variable (a latent variable not influenced by other variables in the model); β_{ji} is the path coefficient between the i-th exogenous latent variable and the j-th endogenous latent variable, optimized through PLS, indicating the degree (equivalent to the standardized regression coefficient) of the response variable relative to the explanatory variable, which facilitates the examination of the direction and strength of causal relationships [34]; ζ_j represents the error in the relationships within the model.

Measurement model (direct effects between variables):

$$X_{jk} = \lambda_{jk}\xi_j + \varepsilon_{jk} \tag{11}$$

where X_{jk} represents the manifest variable; ξ_j is the latent variable; λ_{jk} indicates the correlation coefficient between the manifest and latent variables estimated using the PLS method; the error term ε_{jk} represents the measurement imprecision [14].

The PLS-SEM provides the path coefficients (β) and coefficient of determination (R^2) for all latent variables. The β reveals the strength and direction of the relationships between latent variables, while the R^2 reflects the predictive accuracy of the model, with values ranging from 0 to 1; a higher value indicates better explanatory power of the model. The classification criteria for R^2 used in this study are: 0.10 (not significant fit), 0.25 (weak fit), 0.50 (moderate fit), 0.75 (high fit), and 1 (very high fit). In this study, the PLS-SEM is constructed using R language and the "PLSPM" package [35], where the measurement and structural models optimized by the PLS method quantify the direct and indirect effects between variables. The direct effect is the direct influence of one latent variable on another, typically represented by the path coefficient (β). The indirect effect, on the other hand, is the influence of one latent variable on another through one or more intermediary variables, usually involving the cumulative effect of multiple path coefficients between latent variables.

3. Results

3.1. Changing Characteristics of Precipitation and Streamflow in the YRB

Statistics from 24 meteorological stations and 4 hydrological stations in the YRB from 1984 to 2014 reveal that the annual average precipitation for the areas above the four hydrological stations (Baise, Chongzuo, Nanning, and Guigang) is 983.08 mm, 1113.56 mm, 1052.32 mm, and 1072.87 mm, respectively. The annual average streamflow for these areas is 256.10 m^3/s, 539.54 m^3/s, 1187.96 m^3/s, and 1444.91 m^3/s, respectively. Both precipitation and streamflow exhibit a negative slope, though the downward trend is not statistically significant ($p < 0.05$) [Figure 3a,c].

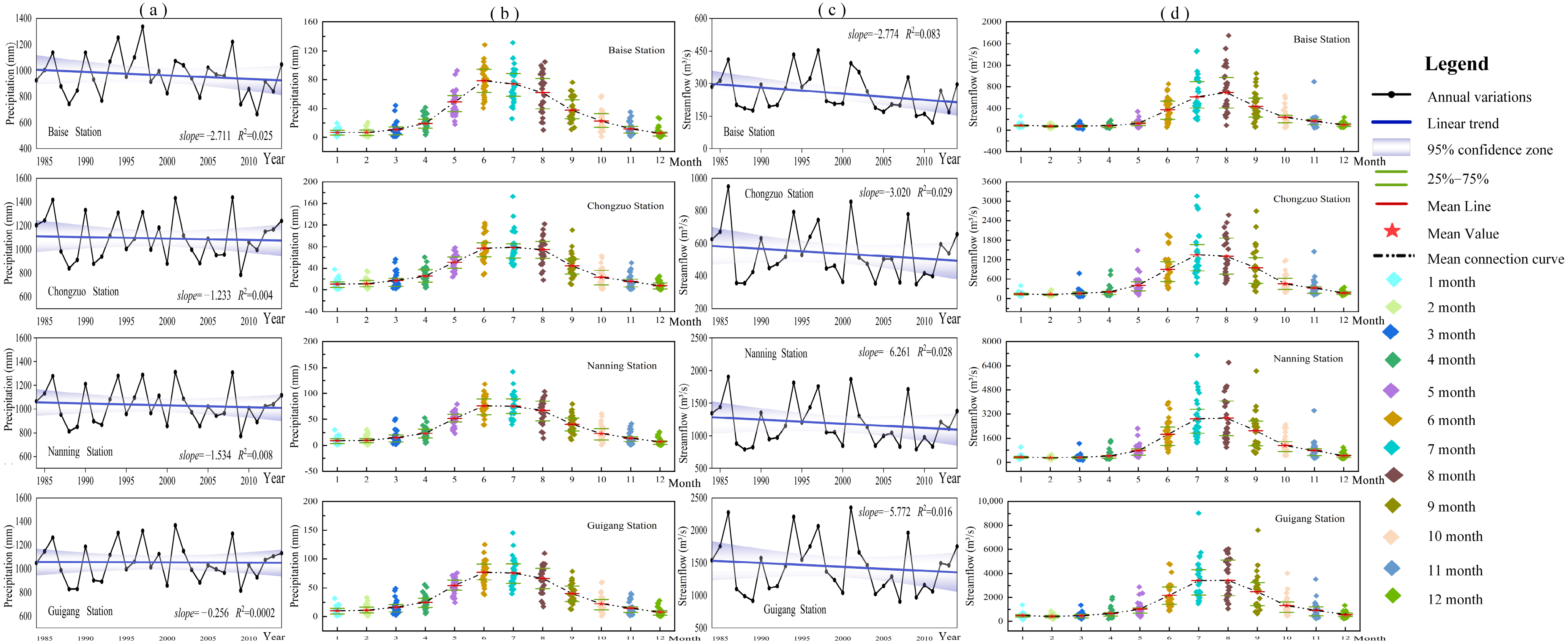

Figure 3. Annual and monthly variations of precipitation and streamflow in the Yujiang River Basin from 1984 to 2014. (**a**) Line chart and trend of annual precipitation; (**b**) Scatter box plot of monthly precipitation; (**c**) Line chart and trend of annual streamflow; (**d**) Scatter box plot of monthly streamflow. In (**b**,**c**), the green horizontal lines represent the range of the 25th to 75th percentiles for the monthly precipitation and streamflow, while the red horizontal lines indicate the long-term average for the monthly precipitation and streamflow.

The maximum precipitation and streamflow values for all four areas occur in July, with a notably uneven distribution throughout the year and significant disparities between wet and dry periods. The variability of precipitation and streamflow is most pronounced between June and September, showing substantial intra-annual variability and uneven distribution. Approximately 60% to 70% of the annual precipitation is concentrated primarily from May to August, while streamflow peaks from June to September, with a slight delay in timing relative to precipitation [Figure 3b,d].

3.2. Changing Characteristics of Meteorological and Hydrological Droughts in the YRB

The methods outlined in Section 3.1 were applied to derive the results presented in Figure 4 and Table 2. As the time scale increases, the SPI values at Baise Station exhibit a decreasing proportion of mild drought duration. In contrast, the pattern observed at Chongzuo, Nanning, and Guigang Stations differs slightly, with the duration of extreme drought decreasing as the time scale increases. Notably, except for the *SPI*-3 and *SPI*-6 at Chongzuo Station and the *SPI*-12 at both Chongzuo and Nanning Stations, the other *SPI* indicators exhibit an upward trend. Additionally, both drought indices (*SPI* and *SSI*) at Baise and Guigang Stations show a reduction in extreme drought duration as the time scale increases, while the duration of mild drought at Nanning Station gradually decreases with the increasing time scale.

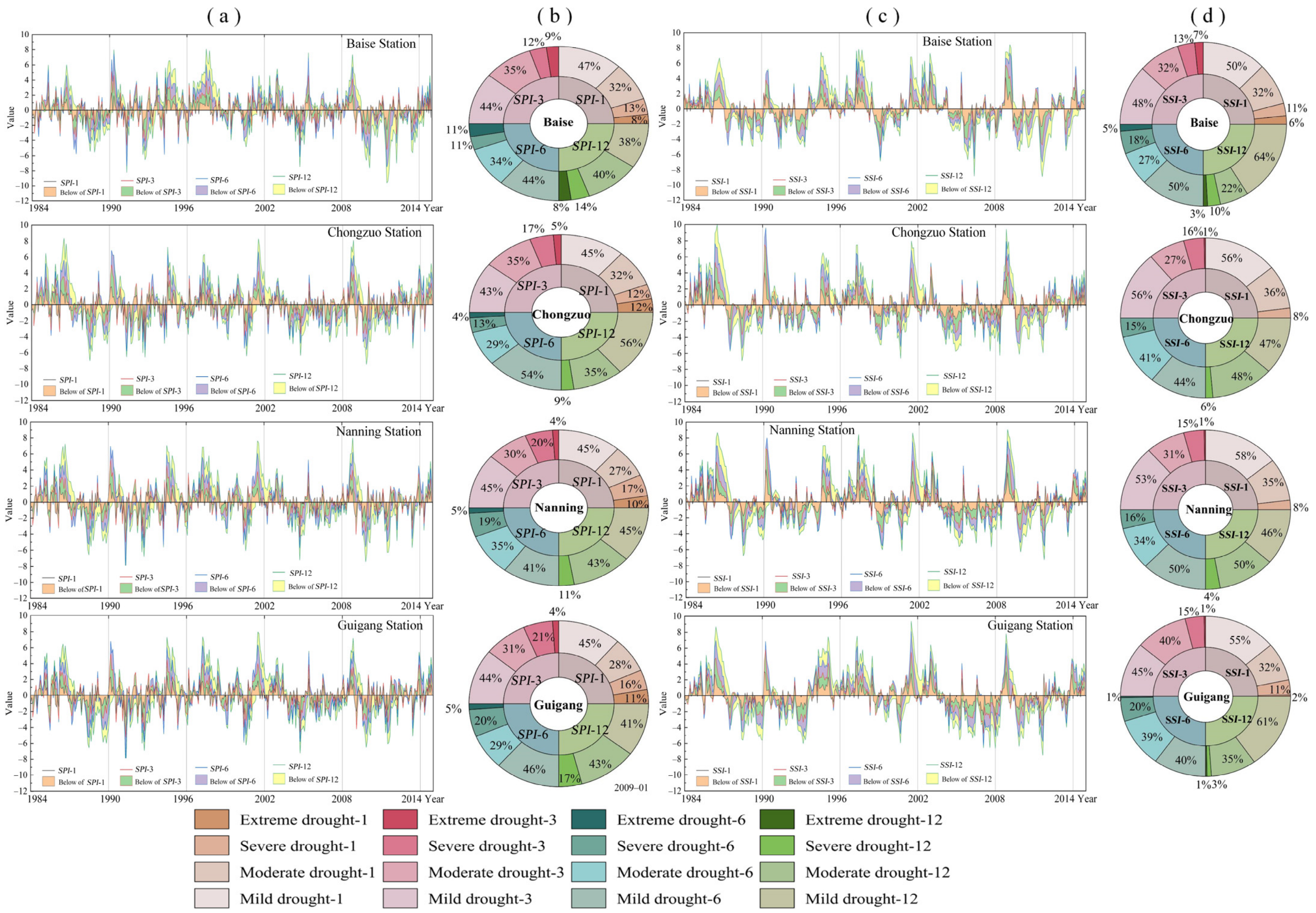

Figure 4. Multi-scale *SPI* and *SSI* variation characteristics in the Yujiang River Basin. (**a**) Cumulative plots of 4 multi-scale *SPI* changes; (**b**) Composition of drought duration proportions of the multi-scale *SPI* series; (**c**) Cumulative plots of 4 multi-scale *SSI* changes; (**d**) Composition of drought duration proportions of the multi-scale *SSI* series.

Table 2. Statistical distribution of drought time proportions for multi-scale *SPI* and *SSI* in the Yujiang River Basin.

Station Name	Meteorological Drought Type					Hydrological Drought Type				
	Index	Mild	Moderate	Severe	Extreme	Index	Mild	Moderate	Severe	Extreme
Baise	*SPI*-1	53	36	15	9	*SSI*-1	56	36	12	7
	SPI-3	50	40	14	10	*SSI*-3	57	38	15	8
	SPI-6	47	36	12	12	*SSI*-6	58	31	21	6
	SPI-12	41	43	15	9	*SSI*-12	89	31	14	4
Chongzuo	*SPI*-1	51	36	13	13	*SSI*-1	68	43	10	0
	SPI-3	50	41	20	6	*SSI*-3	66	32	19	1
	SPI-6	64	34	15	5	*SSI*-6	49	46	17	0
	SPI-12	76	48	12	0	*SSI*-12	57	58	7	0
Nanning	*SPI*-1	48	29	18	11	*SSI*-1	76	46	10	0
	SPI-3	51	34	23	5	*SSI*-3	62	36	18	1
	SPI-6	44	38	21	5	*SSI*-6	62	43	20	0
	SPI-12	55	53	14	0	*SSI*-12	62	66	5	0
Guigang	*SPI*-1	50	31	18	12	*SSI*-1	69	40	14	2
	SPI-3	51	36	25	5	*SSI*-3	55	49	18	1
	SPI-6	50	31	22	5	*SSI*-6	49	48	24	1
	SPI-12	49	51	20	0	*SSI*-12	88	50	5	1

Note: The two columns of trends are not significant at the 0.05% confidence level.

The proportion of drought duration for the two drought indices at these four stations reflects an overall pattern characterized by mild drought > moderate drought > severe drought > extreme drought. Moreover, changes in *SPI* are more pronounced at the same scale compared with *SSI*. As the time scale increases, both SPI and SSI values tend toward stabilization.

Using the run theory described in Section 3.2, the multi-scale SPI and SSI values for the four sites were analyzed to determine the temporal and spatial distribution patterns of meteorological and hydrological drought events (see Figure 5 and Table 3). For meteorological droughts, Baise Station exhibits the highest frequency of moderate drought events across all four *SPI* scales. At Chongzuo Station, *SPI*-1 records the highest number of mild and moderate drought events, each occurring 11 times. *SPI*-3 at this station is dominated by moderate drought events, while *SPI*-6 shows the highest frequency of both mild and moderate drought events, each occurring 9 times. *SPI*-12, however, records the most frequent mild drought events at Chongzuo Station. At Nanning Station, *SPI*-12 records the highest number of mild drought events, while moderate drought events are most common in *SPI*-1, *SPI*-3, and *SPI*-6. Guigang Station records the highest number of mild and moderate drought events in *SPI*-1, with 10 events each. Moderate drought events are most frequent in *SPI*-3 and *SPI*-6 at this station, while *SPI*-12 also records a notable number of mild drought events. The longest continuous meteorological drought events recorded at the four stations are moderate droughts in *SPI*-12. The most severe drought intensities are observed at different scales: *SPI*-12 for Baise Station, *SPI*-3 for Chongzuo Station, *SPI*-1 for Nanning Station, and *SPI*-1 for Guigang Station. Extreme drought events are only recorded at Baise Station in *SPI*-12, Chongzuo Station in *SPI*-3, Nanning Station in *SPI*-1, and Guigang Station in *SPI*-1. No extreme drought events are observed at the other stations across the analyzed *SPI* scales.

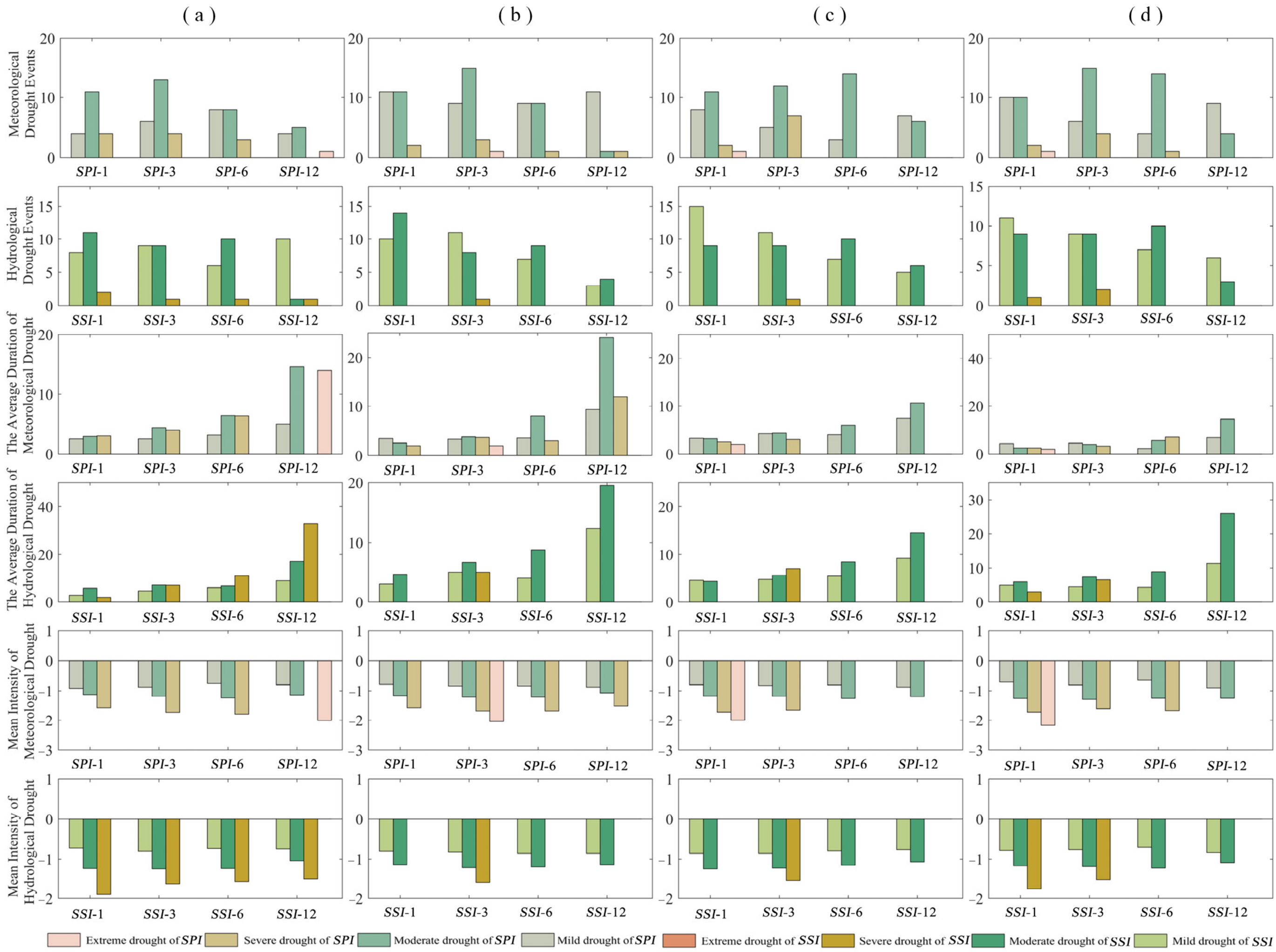

Figure 5. Distribution patterns of multi-scale *SPI* and *SSI* drought events for the stations of (**a**) Baise, (**b**) Chongzuo, (**c**) Nanning, and (**d**) Guigang in the Yujiang River Basin.

For hydrological drought, Baise Station records the highest number of moderate drought events for *SSI*-1 and *SSI*-6, while *SSI*-3 has an equal number of mild and moderate drought events (both 9 events), and *SSI*-12 is primarily characterized by mild drought events. Similarly, Chongzuo Station shows the highest frequency of moderate drought events in *SSI*-1, *SSI*-6, and *SSI*-12, whereas *SSI*-3 is predominantly characterized by mild drought events. At Nanning Station, there is a notable number of mild drought events for *SSI*-1 and *SSI*-3, with a high frequency of moderate drought events for *SSI*-6 and *SSI*-12. Similarly, Guigang Station experiences a relatively high frequency of mild drought events in *SSI*-1 and *SSI*-12, with *SSI*-3 showing equal occurrences of mild and moderate drought events (both 9 events), and *SSI*-6 recording a larger number of moderate drought events. The longest duration of hydrological drought events at Baise Station is recorded for a severe drought event in *SSI*-12, while the longest duration at the other three stations is for moderate drought events in *SSI*-12. The drought intensity is most severe for Baise Station's *SSI*-1, Chongzuo and Guigang Stations' *SSI*-6, and Nanning Station's *SSI*-3. None of the four stations records extreme-drought events across the four scales of hydrological drought monitoring.

Overall, at the same timescale, the number of drought events detected by the *SPI* is generally higher than that detected by the *SSI*, indicating greater sensitivity to meteorological drought. As the timescale increases, the number of drought events detected by both *SPI* and *SSI* gradually decreases. Among the four stations, *SPI*-3 and *SSI*-1 record a relatively higher number of drought events, suggesting that the optimal timescales for characterizing meteorological and hydrological drought in the YRB are 3 months and 1 month, respectively. However, the average duration and intensity of drought events do not exhibit a consistent pattern, with significant variability observed among the stations.

Table 3. Statistical results of multi-scale *SPI* and *SSI* drought events in the Yujiang River Basin.

Station Name	Index	Drought Events	The Average Duration of Drought (Month)	Mean Intensity of Drought	Drought Type	Index	Drought Events	The Average Duration of Drought (Month)	Mean Intensity of Drought	Drought Type
Baise	*SPI*-1	19	2.84	−1.20	Moderate	*SSI*-1	21	4.29	−1.10	Moderate
	SPI-3	23	3.83	−1.21	Moderate	*SSI*-3	19	5.95	−1.05	Moderate
	SPI-6	19	5.00	−1.13	Moderate	*SSI*-6	17	6.71	−1.07	Moderate
	SPI-12	10	10.70	−1.10	Moderate	*SSI*-12	12	11.58	−0.84	Mild
Nanning	*SPI*-1	24	2.92	−1.03	Moderate	*SSI*-1	24	3.96	−1.00	Moderate
	SPI-3	28	3.57	−1.18	Moderate	*SSI*-3	20	5.65	−1.02	Moderate
	SPI-6	19	5.63	−1.04	Moderate	*SSI*-6	16	6.69	−1.06	Moderate
	SPI-12	13	10.69	−0.87	Mild	*SSI*-12	7	16.43	−1.00	Moderate
Chongzuo	*SPI*-1	22	3.09	−1.17	Moderate	*SSI*-1	24	4.46	−0.99	Mild
	SPI-3	24	3.92	−1.27	Moderate	*SSI*-3	21	5.19	−1.03	Moderate
	SPI-6	17	5.65	−1.18	Moderate	*SSI*-6	17	7.18	−1.00	Mild
	SPI-12	13	8.92	−0.98	Mild	*SSI*-12	11	12.09	−0.95	Mild
Guigang	*SPI*-1	23	3.26	−1.12	Moderate	*SSI*-1	21	5.24	−0.99	Mild
	SPI-3	25	3.96	−1.23	Moderate	*SSI*-3	20	5.95	−1.01	Moderate
	SPI-6	19	4.95	−1.13	Moderate	*SSI*-6	17	7.00	−1.02	Moderate
	SPI-12	13	9.15	−0.93	Mild	*SSI*-12	9	16.22	−0.92	Mild

3.3. Correlation Between Meteorological and Hydrological Droughts at the Same Time Scale

The PLS-SEM can effectively measure the driving relationships between observable variables and latent variables that cannot be directly observed. The output of this model shows that the total effect between any two variables is composed of the sum of direct effects and indirect effects, where direct effects are determined by the corresponding path coefficients, and indirect ones involve intermediate variables. This study uses the PLS-SEM to explore the correlation between hydrological and meteorological droughts at the same time scale for four time scales (i.e., 1, 3, 6, and 12 months). The results are shown in Figure 6 and Table 4. In Figure 6, the ellipses represent latent variables; rectangles represent the observable variables corresponding to the latent variables. The numbers on the arrows between the latent variables and their observable variables indicate loadings, while the numbers on the other arrows represent path coefficients, which also indicate causal relationships. Solid arrows indicate positive correlations, while dashed arrows indicate negative correlations. The arrows between latent variables represent causal relationships, indicating that the former influences or predicts the latter. The arrows between latent variables and their corresponding observable variables indicate measurement relationships, showing that observable variables are indicators or manifestations of latent variables.

The R^2 values for *SPI*-1 and *SSI*-1 at four hydrological stations indicate moderate predictive accuracy, with *SSI*-1 being slightly more accurate than *SPI*-1. The large-scale teleconnection climate indices and meteorological factors exhibit weak positive indirect correlations with both *SPI*-1 and *SSI*-1. Precipitation shows a strong positive direct effect on *SPI*-1 and a weak negative direct effect on *SSI*-1, but a strong positive indirect effect on both, resulting in an overall positive correlation. Streamflow has a weak direct effect on *SPI*-1 but a strong direct effect on *SSI*-1. Land cover has a strong negative correlation with both *SPI*-1 and *SSI*-1 ($p < 0.05$). Precipitation explains 75–80% of the variability in *SPI*-1, while streamflow explains 80–97% of the variability in *SSI*-1. Thus, precipitation is the dominant driver of *SPI*-1, while streamflow strongly influences *SSI*-1.

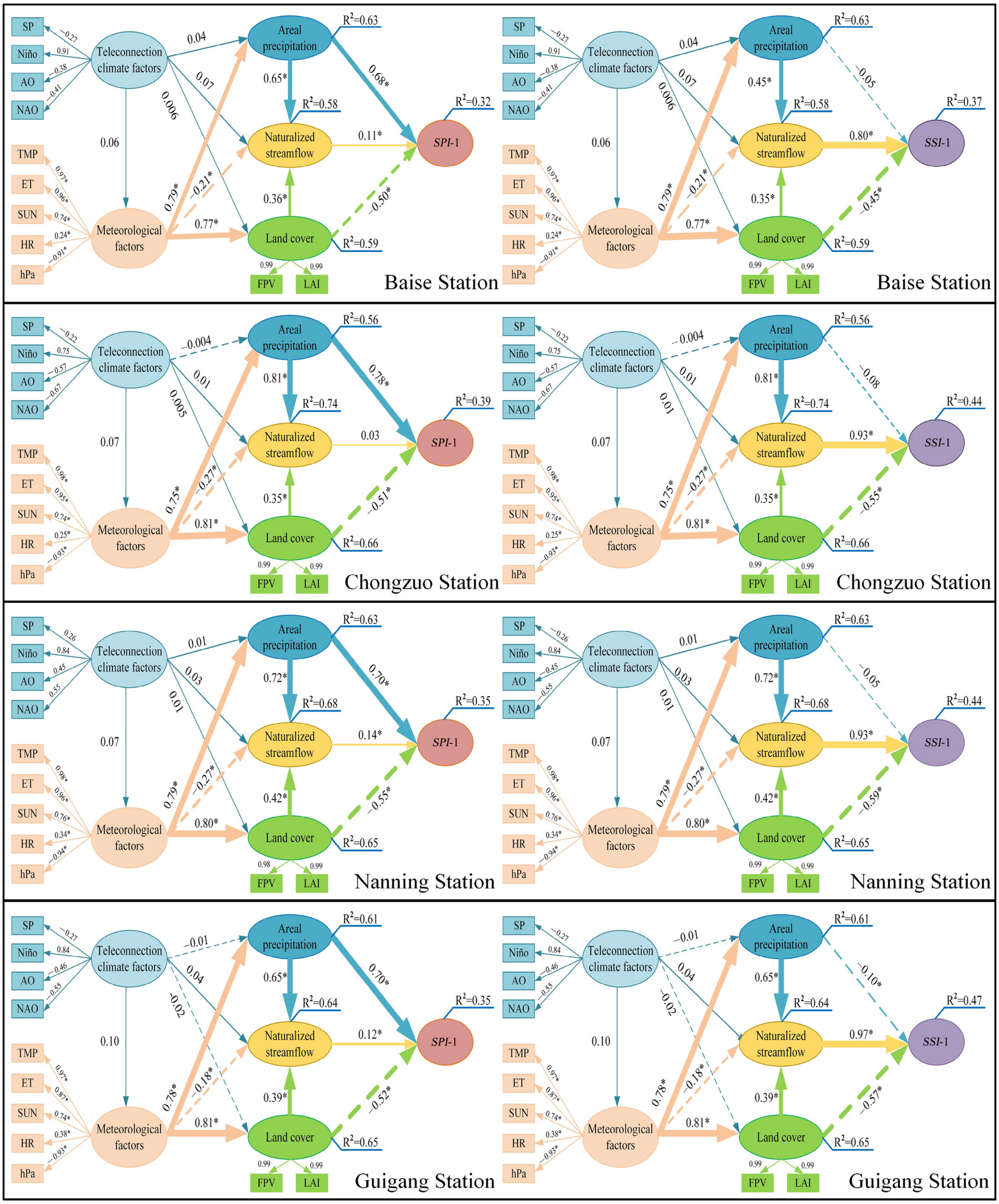

(**a**)

Figure 6. *Cont.*

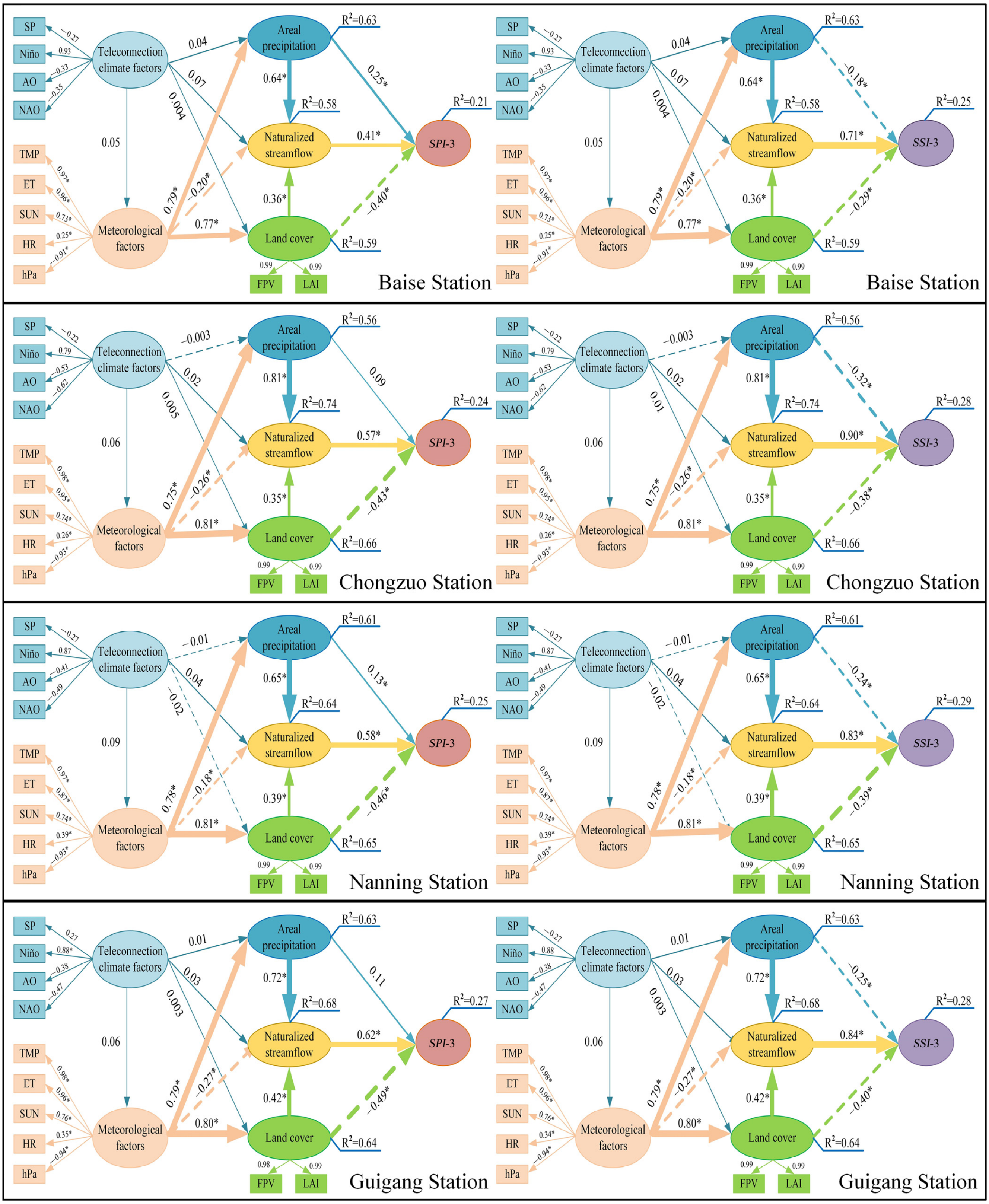

(**b**)

Figure 6. *Cont*.

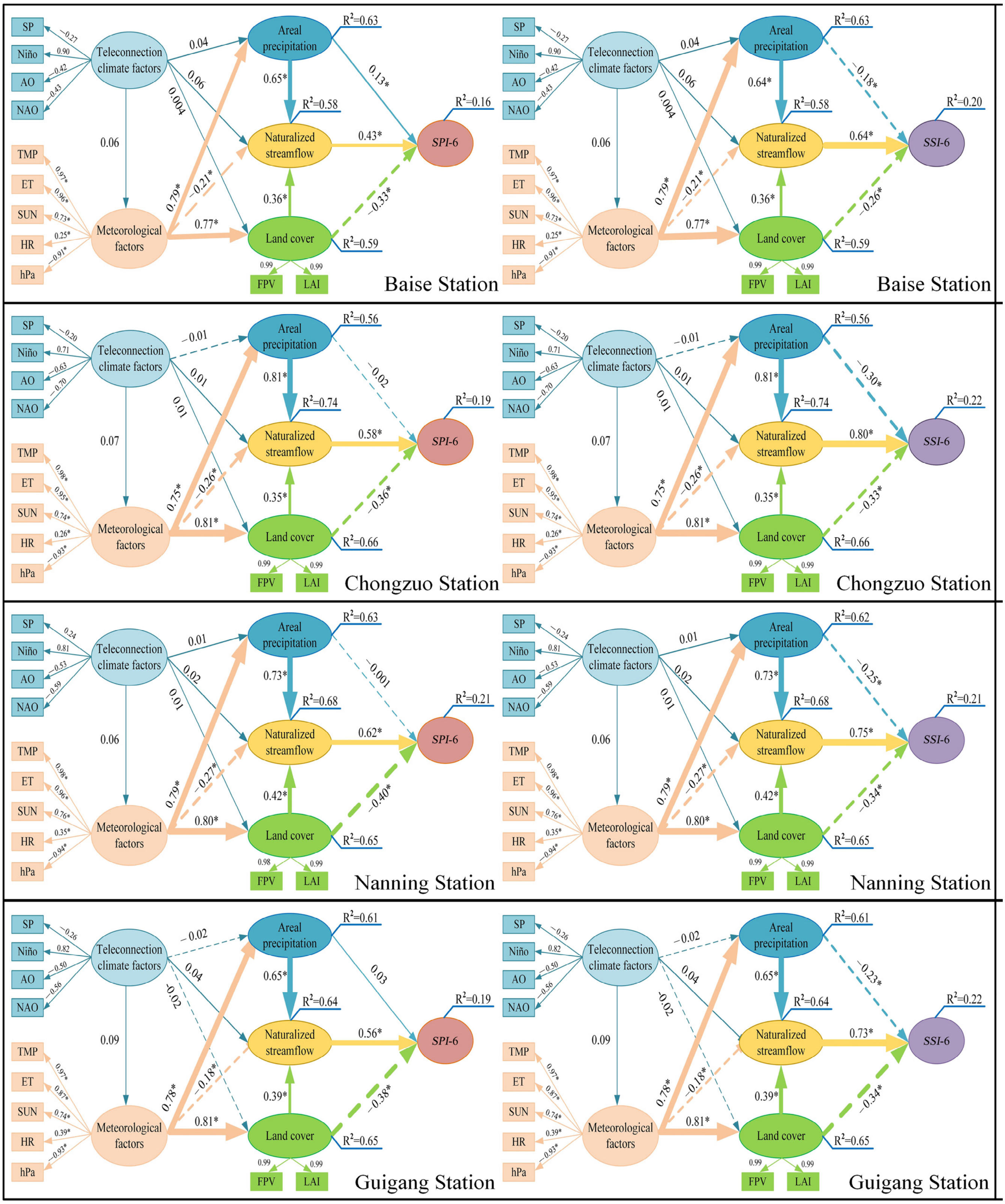

(**c**)

Figure 6. *Cont.*

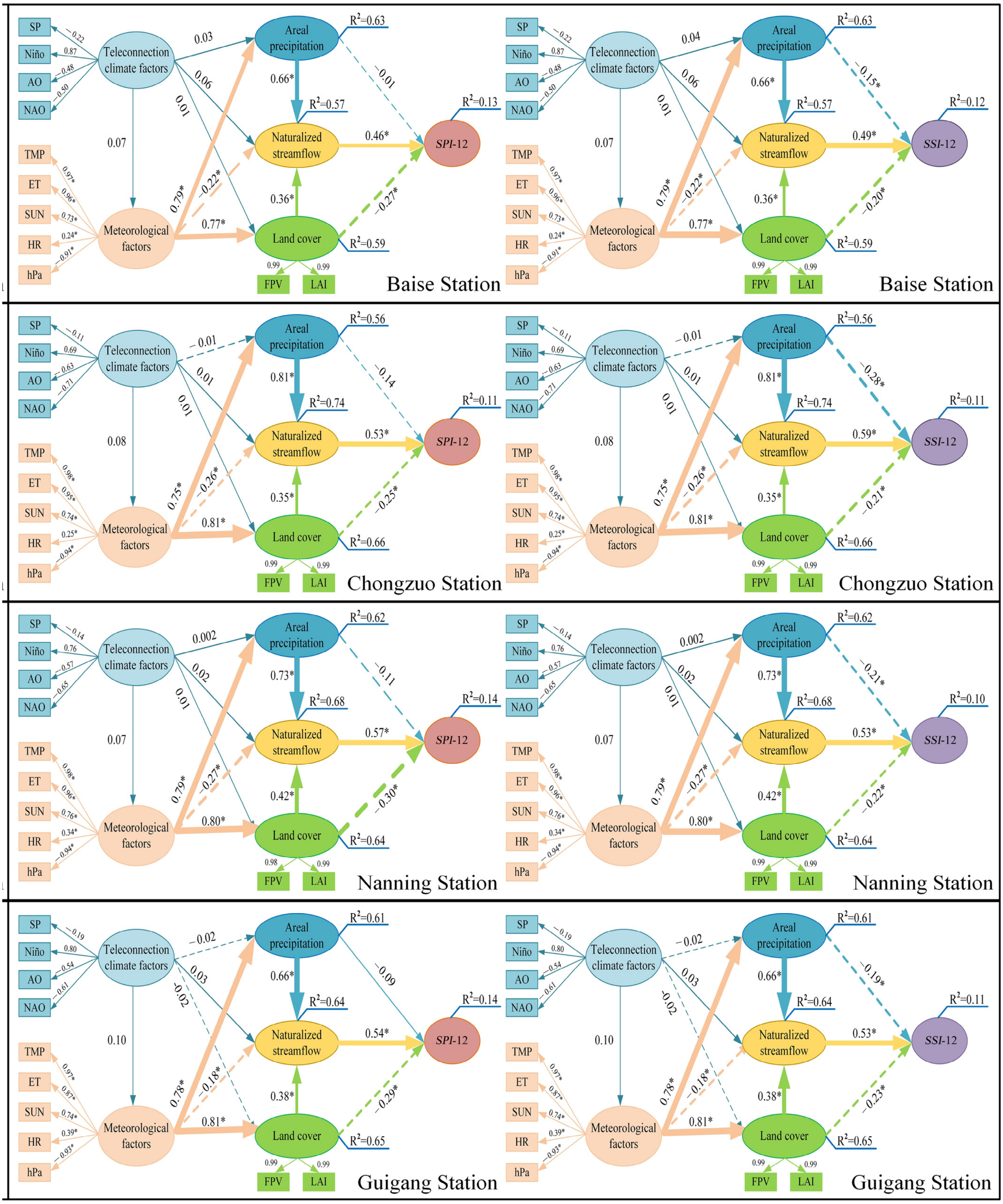

(**d**)

Figure 6. Results of PLS-SEM for *SPI* and *SSI* at different scales of (**a**) 1 month, (**b**) 3 months, (**c**) 6 months, and (**d**) 12 months in the Yujiang River Basin. The symbol "*" indicates explicit correlation ($p < 0.05$). SP: Sunspot; Niño: Ocean Niño; AO: Arctic Oscillation; NAO: North Atlantic Oscillation; TEM: air temperature; ET: evapotranspiration; SUN: sunshine duration; HR: relative humidity; hPa: atmospheric pressure; FPV: photosynthetic vegetation fractional cover; LAI: leaf area index.

Table 4. PLS-SEM results of *SPI* and *SSI* at multiple scales (1, 3, 6 and 12) in Yujiang River Basin.

Latent Variables	Hydrological Station	Direct Impact	Indirect Impact	Total	Direct Impact	Indirect Impact	Total	Direct Impact	Indirect Impact	Total	Direct Impact	Indirect Impact	Total
		***SPI*-1**			***SSI*-1**			***SPI*-3**			***SSI*-3**		
Teleconnection climate factors	Baise	N.A	0.05	0.05	N.A	0.06	0.06	N.A	0.05	0.05	N.A	0.06	0.06
Meteorological factors		N.A	0.22	0.22	N.A	−0.05	−0.05	N.A	0.13	0.13	N.A	0.05	0.05
Areal precipitation		0.68	0.07	0.75	−0.05	0.36	0.31	0.25	0.26	0.51	−0.18	0.45	0.27
Naturalized streamflow		0.11	N.A	0.11	0.80	N.A	0.80	0.41	N.A	0.41	0.71	N.A	0.71
Land cover		−0.50	0.04	−0.46	−0.45	0.28	−0.17	−0.40	0.15	−0.25	−0.29	0.26	−0.03
Teleconnection climate factors	Chongzuo	N.A	0.01	0.01	N.A	0.01	0.01	N.A	0.01	0.01	N.A	0.02	0.02
Meteorological factors		N.A	0.19	0.19	N.A	0.07	0.07	N.A	0.08	0.08	N.A	0.02	0.02
Areal precipitation		0.78	0.02	0.8	−0.08	0.75	0.67	0.09	0.46	0.55	−0.32	0.73	0.41
Naturalized streamflow		0.03	N.A	0.03	0.93	N.A	0.93	0.57	N.A	0.57	0.90	N.A	0.90
Land cover		−0.51	0.01	−0.5	−0.55	0.33	−0.22	−0.43	0.2	−0.23	−0.38	0.32	−0.07
Teleconnection climate factors	Nanning	N.A	0.02	0.02	N.A	0.04	0.04	N.A	0.03	0.03	N.A	0.03	0.03
Meteorological factors		N.A	0.20	0.20	N.A	0.08	0.08	N.A	0.09	0.09	N.A	0.02	0.02
Areal precipitation		0.70	0.10	0.80	−0.05	0.67	0.62	0.11	0.45	0.56	−0.25	0.60	0.35
Naturalized streamflow		0.14	N.A	0.14	0.93	N.A	0.93	0.62	N.A	0.62	0.84	N.A	0.84
Land cover		−0.55	0.06	−0.49	−0.59	0.39	−0.20	−0.49	0.26	−0.23	−0.4	0.35	−0.05
Teleconnection climate factors	Guigang	N.A	0.03	0.03	N.A	0.05	0.05	N.A	0.03	0.03	N.A	0.03	0.03
Meteorological factors		N.A	0.20	0.20	N.A	0.08	0.08	N.A	0.10	0.10	N.A	0.03	0.03
Areal precipitation		0.70	0.08	0.78	−0.10	0.63	0.53	0.13	0.38	0.51	−0.24	0.54	0.30
Naturalized streamflow		0.12	N.A	0.12	0.97	N.A	0.97	0.58	N.A	0.58	0.83	N.A	0.83
Land cover		−0.52	0.05	−0.47	−0.57	0.38	−0.19	−0.46	0.23	−0.23	−0.39	0.32	−0.07
Latent variables	**Hydrological station**	***SPI*-6**			***SSI*-6**			***SPI*-12**			***SSI*-12**		
Teleconnection climate factors	Baise	N.A	0.05	0.05	N.A	0.05	0.05	N.A	0.04	0.04	N.A	0.04	0.04
Meteorological factors		N.A	0.10	0.10	N.A	0.02	0.02	N.A	0.05	0.05	N.A	0.01	0.01
Areal precipitation		0.13	0.28	0.41	−0.18	0.41	0.23	−0.01	0.30	0.29	−0.15	0.32	0.17
Naturalized streamflow		0.43	N.A	0.43	0.64	N.A	0.64	0.46	N.A	0.46	0.49	N.A	0.49
Land cover		−0.33	0.15	−0.18	−0.26	0.23	−0.03	−0.27	0.17	−0.10	−0.2	0.18	−0.02
Teleconnection climate factors	Chongzuo	N.A	0.00	0.00	N.A	0	0	N.A	0.00	0.00	N.A	0.00	0.00
Meteorological factors		N.A	0.06	0.06	N.A	0.01	0.01	N.A	0.03	0.03	N.A	−0.01	−0.01
Areal precipitation		−0.02	0.47	0.45	−0.30	0.65	0.35	−0.14	0.43	0.29	−0.28	0.48	0.2
Naturalized streamflow		0.58	N.A	0.58	0.80	N.A	0.80	0.53	N.A	0.53	0.59	N.A	0.59
Land cover		−0.36	0.20	−0.16	−0.33	0.28	−0.05	−0.25	0.19	−0.06	−0.21	0.21	0.00
Teleconnection climate factors	Nanning	N.A	0.02	0.02	N.A	0.02	0.02	N.A	0.01	0.01	N.A	0.01	0.01
Meteorological factors		N.A	0.08	0.08	N.A	0.01	0.01	N.A	0.04	0.04	N.A	0.00	0.00
Areal precipitation		0.00	0.45	0.45	−0.25	0.55	0.30	−0.11	0.42	0.31	−0.21	0.39	0.18
Naturalized streamflow		0.62	N.A	0.62	0.75	N.A	0.75	0.57	N.A	0.57	0.53	N.A	0.53
Land cover		−0.40	0.26	−0.14	−0.34	0.32	−0.03	−0.30	0.24	−0.06	−0.22	0.22	0.00

Table 4. *Cont.*

Latent Variables	Hydrological Station	*SPI*-1			*SSI*-1			*SPI*-3			*SSI*-3		
		Direct Impact	Indirect Impact	Total	Direct Impact	Indirect Impact	Total	Direct Impact	Indirect Impact	Total	Direct Impact	Indirect Impact	Total
Teleconnection climate factors	Guigang	N.A	0.02	0.02	N.A	0.03	0.03	N.A	0.02	0.02	N.A	0.01	0.01
Meteorological factors		N.A	0.08	0.08	N.A	0.01	0.01	N.A	0.04	0.04	N.A	0.01	0.01
Areal precipitation		0.03	0.36	0.39	−0.23	0.47	0.24	−0.09	0.36	0.27	−0.19	0.35	0.16
Naturalized streamflow		0.56	N.A	0.56	0.73	N.A	0.73	0.54	N.A	0.54	0.53	N.A	0.53
Land cover		−0.38	0.22	−0.16	−0.34	0.28	−0.06	−0.29	0.21	−0.08	−0.23	0.20	−0.03

For *SPI*-3 and *SSI*-3, the R^2 values indicate weaker predictive accuracy compared with *SPI*-1 and *SSI*-1. The influence of large-scale climate indices and meteorological factors remains weak. Precipitation has a strong positive correlation with *SPI*-3 and a weak negative direct effect on *SSI*-3, but a strong positive indirect effect. Streamflow has a positive direct influence on both *SPI*-3 and *SSI*-3, with a stronger effect on *SSI*-3. Land cover shows a negative direct and positive indirect influence on both, resulting in an overall negative correlation.

The R^2 values for *SPI*-6 and *SSI*-6 indicate weak predictive accuracy. The effects of large-scale climate indices and meteorological factors remain weak. Precipitation has a weak positive direct effect on *SPI*-6 and a weak negative direct effect on *SSI*-6, but strong positive indirect effects on both. Streamflow has a positive direct effect on both models, with the strongest influence on *SSI*-6. Land cover has a negative direct and positive indirect effect on both, resulting in an overall negative correlation. The influence of variables on *SPI*-6 ranks as: streamflow > precipitation > land cover > meteorological factors > climate indices. For *SSI*-6, streamflow has the strongest influence, while climate indices and meteorological factors have the least.

Finally, the R^2 values for *SPI*-12 and *SSI*-12 indicate weak predictive accuracy. The effects of climate indices and meteorological factors are slight but positive. Precipitation has a weak negative direct effect and a strong positive indirect effect on both *SPI*-12 and *SSI*-12. Streamflow has a strong positive direct effect on both models. Land cover has a strong negative direct effect and a weak positive indirect effect on both, resulting in an overall negative correlation. Streamflow is the strongest driver of both *SPI*-12 and *SSI*-12, while climate indices and meteorological factors have the least influence.

3.4. Lag Response Time Between Hydrological and Meteorological Droughts

The hydrological regulation and storage functions of a watershed's underlying surface and river channels explain why not all meteorological droughts develop into hydrological droughts, and why hydrological droughts may not necessarily be triggered by meteorological droughts. The time required for drought propagation quantitatively reflects the lagged response between meteorological and hydrological droughts. This study employs Pearson correlation analysis to quantify the optimal correlation between meteorological and hydrological droughts at four timescales in the YRB, thereby determining the lag response time of droughts. The results reveal the strongest Pearson correlations between *SSI*-1 and *SPI*-3, *SSI*-3 and *SPI*-6, *SSI*-6 and *SPI*-6, and *SSI*-12 and *SPI*-12 (Figure 7). Consequently, the optimal response times for hydrological droughts relative to meteorological droughts at the 1-, 3-, 6-, and 12-month scales are 2, 3, 1, and 1 months, respectively, indicating a lag of 1–3 months between hydrological and meteorological droughts in the YRB. The lag effect of meteorological drought propagating to hydrological drought is strongest at Nanning Station, followed by Chongzuo, Guigang, and Baise Stations.

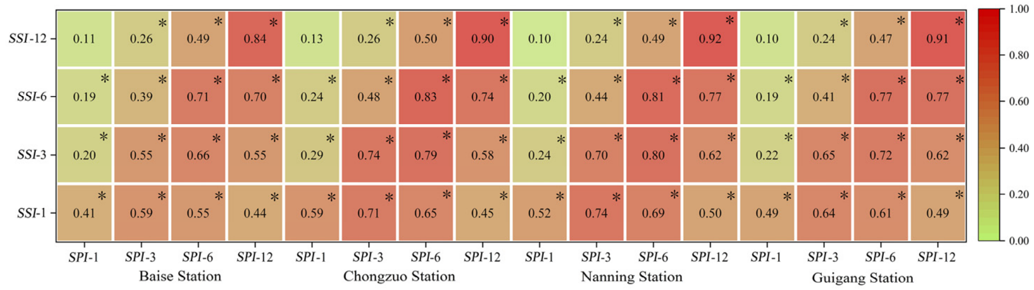

Figure 7. Lag results of multi-scale *SPI* and *SSI* in Yujiang River Basin. * indicates an explicit correlation ($p < 0.05$).

4. Discussion

4.1. Distribution Patterns of Different Types of Multi-Scale Droughts in the YRB

The YRB is characterized by fragile karst topography and strong surface water retention capacity, which exacerbate the occurrence and propagation of drought phenomena within the basin. Consequently, the spatial and temporal distribution of droughts in this region exhibits a high degree of irregularity. Over the 30-year period from 1984 to 2014, precipitation and streamflow at the four hydrological stations (Baise, Nanning, Chongzuo, and Guigang) show a gradual downward trend [Figure 3a]. The annual distribution of precipitation and streamflow is uneven, with intra-annual variability also being unstable [Figure 3b,d]. Drought events at different time scales across the stations generally follow the pattern of mild drought > moderate drought > severe drought > extreme drought. At the same time scale, the trend of the *SPI* is more pronounced than that of the *SSI*. As the time scale increases, the changes in both *SPI* and *SSI* become more gradual [Figure 4a,c]. Figure 4b,c reveal that the frequency of extreme drought events at the upstream Baise station is relatively high, with more severe drought intensity, consistent with [20], who concluded that "the frequency of hydrological droughts in the Xijiang River is continuously increasing, with a trend of reduced drought severity from upstream to downstream." Similar findings were reported by [36].

The results of the multi-site and multi-scale *SPI* and *SSI* sequences analyzed using run theory (Figure 5) indicate that, at the same scale, the number of drought events detected by *SPI* is greater than those detected by *SSI*. The event count, intensity, and duration of meteorological drought are significantly higher than those of hydrological drought (Figure 5), aligning with the findings of [37], who demonstrates that meteorological drought monitoring is more sensitive to water deficiency conditions than hydrological drought monitoring. As the time scale increases, the number of drought events detected at the four hydrological stations is highest for *SPI*-3, suggesting that the optimal scale for monitoring meteorological drought is 3 months. Conversely, the SSI values at the four sites decrease sequentially with increasing scale, indicating that the optimal scale for monitoring hydrological drought is 1 month (*SSI*-1). However, the intensity and duration of droughts for *SPI* and *SSI* at different sites and scales do not exhibit a uniform pattern (Figure 5 and Table 3). Due to the watershed's regulating effects (hydrological regulation and storage function), a quantitative analysis using Pearson correlation coefficients reveals that the optimal response times of hydrological drought to meteorological drought at 1-, 3-, 6-, and 12-month scales are 2 months, 3 months, 1 month, and 1 month, respectively. This indicates a lag of 1 to 3 months for hydrological drought compared with meteorological drought in the YRB (Figure 7). Therefore, assessing the spatiotemporal dynamics of meteorological and hydrological drought not only enhances our understanding of their changing characteristics but also improves regional drought monitoring capabilities, thereby mitigating adverse impacts. These findings provide critical theoretical support for future drought prevention and mitigation strategies, ecological restoration projects, and the development of ecological civilization.

4.2. Complex Coupling Response Mechanism of Hydrometeorological Droughts

Drought can be triggered by extreme phenomena in natural climate variability, which are linked to interactions within the atmosphere and feedback mechanisms from ocean and land surfaces [5]. Previous studies (e.g., [38–41]) have focused on the quantitative analysis of individual driving factors affecting drought. However, these studies often fail to distinguish between the direct and indirect impacts of large-scale teleconnection climate indices, meteorological factors, land cover, areal precipitation, and naturalized streamflow on drought. Additionally, they have overlooked the differences in how these five categories of variables influence various types of drought at multiple scales in the YRB. The PLS-SEM approach is a robust method for exploring and testing hypotheses about system relationships [42]. By analyzing the structural model [Equation (10)] and measurement model [Equation (11)] of PLS-SEM, it is possible to more intuitively and accurately assess the direct and indirect effects of different latent variables on multi-scale drought in the YRB.

The teleconnection of large-scale climate indices with other potential variables exhibits a weak positive correlation (Figure 6). This is attributed to the intensity of solar activity, which influences the hydrological cycle and, in turn, affects the occurrence of global climate droughts and other extreme events [43]. The El Niño phenomenon, Arctic Oscillation, and North Atlantic Oscillation all impact the variability of marine climate within large-scale regions [44], thereby producing lagged effects on regional meteorological and hydrological characteristics. Furthermore, drought events are also influenced by teleconnection atmospheric circulation [21,45,46]. Meteorological factors show a strong positive correlation with areal precipitation and an even stronger positive correlation with naturalized streamflow (Figure 6). Meteorological factors significantly influence surface land cover [47], primarily because they can reduce the total energy transfer to the atmosphere [11], thereby decreasing precipitation and increasing the risk of drought through soil-precipitation feedback mechanisms [48]. The strong positive correlation of meteorological factors with land cover is consistent with the conclusion drawn by [10] that meteorological factors positively influence vegetation coverage. Areal precipitation and naturalized streamflow exhibit a strong positive correlation, while areal precipitation also shows a strong positive correlation with meteorological drought (*SPI*) and primarily exhibits a strong positive correlation with hydrological drought (*SSI*) (Figure 6). This phenomenon is closely related to the long-term relationships between drought, precipitation, and streamflow [49]. Severe climate changes may lead to anticyclonic conditions such as clear skies, increased surface radiation, and rising air temperatures, which enhance regional potential evapotranspiration, altering precipitation patterns and streamflow processes in watersheds [50], significantly impacting local water resource management. Naturalized streamflow shows a strong positive correlation with meteorological drought (*SPI*) and an even stronger positive correlation with hydrological drought (*SSI*) (Figure 6). In long-term water-scarce environments, reductions in precipitation can significantly amplify changes in streamflow, typically resulting in a 2–3-fold decrease in streamflow due to reduced precipitation [51]. Therefore, during drought periods, the magnitude of streamflow reduction tends to increase over time [52,53], making its response to hydrological drought more sensitive.

This study conducts a comprehensive analysis of the complex driving mechanisms behind multi-scale meteorological and hydrological droughts from five perspectives: teleconnection of large-scale climate indices, meteorological factors, land cover, areal precipitation, and naturalized streamflow. The results reveal significant spatial differences in the response mechanisms of the *SPI* and *SSI* at the same scale; while at different scales, the response mechanisms between *SPI* and *SSI* exhibit clear temporal and spatial variation patterns (as shown in Figure 6 and Table 4). This indirectly supports the decisive role of precipitation in regional wet and dry changes [45]. The relationship between precipitation and streamflow is largely regulated by the interaction between soil moisture and the atmosphere [12]. Under specific drought conditions, the relationship between precipitation and streamflow may also change [54,55], making the impact of streamflow on meteorological and hydrological droughts between regions more complex. Although the correlation of land cover with meteorological and hydrological droughts weakens as the time scale increases, at the same scale, the impact of land cover on meteorological drought significantly strengthens (Figure 6 and Table 4). This can be attributed to the distinctive ecohydrological processes of karst basins. In the YRB, vegetation can intercept precipitation and enhance evapotranspiration, thereby reducing the amount of water available for soil moisture recharge and runoff generation. Meanwhile, the shallow soils, high permeability, and well-developed fractures of karst terrains facilitate rapid infiltration and strengthen subsurface hydrological connectivity, allowing vegetation to further regulate groundwater flow and subsurface runoff through root-system effects. Therefore, the negative effect of land cover on drought indices reflects not only vegetation water consumption, but also its role in redistributing precipitation and modifying surface–subsurface hydrological pathways, which together constrain effective water availability and amplify drought responses in the YRB [21,56,57].

Overall, the results provide insights into the multi-factor coupling mechanisms of drought evolution in the Yujiang River Basin. It should be noted that the PLS-SEM framework assumes linear relationships among variables, whereas drought responses may exhibit nonlinear characteristics. Future studies could explore nonlinear approaches to further improve the understanding of drought dynamics.

5. Conclusions

This study investigates the complex coupling response mechanisms of multi-scale drought to teleconnection climate indices, meteorological factors, areal precipitation, naturalized streamflow, and land cover in the YRB of Southern China over a 30-year period (1984–2014). The findings reveal significant insights into the dynamics of meteorological and hydrological droughts, offering valuable implications for drought management and water resource planning. The main conclusions are as follows:

(i) The study demonstrates a gradual decline in precipitation and streamflow in the YRB, accompanied by a decreasing frequency of drought events across all severity levels (mild to extreme). *SPI*-3 (3-month scale) is identified as the optimal monitoring scale for meteorological drought, while *SSI*-1 (1-month scale) is optimal for hydrological drought. These findings provide a robust framework for selecting appropriate drought monitoring scales in similar regions.

(ii) The study identifies a lag of 1 to 3 months between meteorological and hydrological droughts in the YRB. This lag is attributed to the hydrological regulation and storage functions of the watershed, which delay the propagation of drought conditions from precipitation to streamflow. The strongest lag effect is observed at the Nanning station, emphasizing the need for integrated approaches to drought management that account for these temporal delays. Understanding this lag is critical for improving early warning systems and ensuring timely responses to drought events.

(iii) The PLS-SEM results reveal a clear hierarchical driving mechanism of meteorological and hydrological droughts. Precipitation and streamflow are identified as the dominant direct drivers of SPI and SSI, respectively, while large-scale climate indices and meteorological factors mainly exert indirect influences through their regulation of precipitation and streamflow. Land cover variables show a consistent negative effect on both drought indices, indicating the important role of vegetation dynamics in modulating drought propagation processes. Overall, these results highlight that drought evolution in the Yujiang River Basin is governed by the combined effects of climatic forcing, hydrological response, and underlying surface conditions, reflecting a complex multi-factor coupling mechanism.

In future work, higher-resolution precipitation datasets and alternative spatial aggregation methods (e.g., interpolation-based approaches) could be incorporated to further improve the representation of precipitation variability at the basin scale. In addition, the influence of different precipitation processing methods on drought propagation deserves further investigation. Moreover, integrating additional hydrological and human activity factors may help to better understand the complex mechanisms governing the interaction between meteorological and hydrological droughts.

Author Contributions: Conceptualization, X.Y. and X.L.; methodology, X.Y. and X.L.; software, X.D.; validation, Y.H. (Yanbing Huang); formal analysis, Y.H. (Yongjun Huang); investigation, J.S.; resources, X.Y.; data curation, Q.Y.; writing—original draft preparation, Y.H. (Yanbing Huang), X.Y. and X.L.; writing—review and editing, X.Y. and X.L.; visualization, Q.Y.; supervision, X.L.; project administration, X.L.; funding acquisition, X.L. All authors have read and agreed to the published version of the manuscript.

Funding: This research was funded by the National Natural Science Foundation of China (Grant No. 52269001) and the Emergency Management Joint Innovation Technology Key Projects (Type I) by Emergency Management Department of Guangxi Zhuang Autonomous Region (Grant No. 2024GXYJ005).

Data Availability Statement: The data will be available on request.

Conflicts of Interest: The authors declare no conflicts of interest.

References

1. Dikshit, A.; Pradhan, B.; Alamri, A.M. Long lead time drought forecasting using lagged climate variables and a stacked long short-term memory model. *Sci. Total Environ.* **2021**, *755*, 142638. [CrossRef]
2. Trenberth, K.E.; Dai, A.; van der Schrier, G.; Jones, P.D.; Barichivich, J.; Briffa, K.R.; Sheffield, J. Global warming and changes in drought. *Nat. Clim. Change* **2024**, *4*, 17–22. [CrossRef]
3. Ault, T.R. On the essentials of drought in a changing climate. *Science* **2020**, *368*, 256–260. [CrossRef]
4. Hayes, M.J.; Svoboda, M.D.; Wiihite, D.A.; Vanyarkho, O.V. Monitoring the 1996 drought using the standardized precipitation index. *Bull. Am. Meteorol. Soc.* **1999**, *80*, 429–438. [CrossRef]
5. Wang, H.; Chen, Y.; Pan, Y.; Li, W. Spatial and temporal variability of drought in the arid region of China and its relationships to teleconnection indices. *J. Hydrol.* **2015**, *523*, 283–296. [CrossRef]
6. Huang, S.; Li, P.; Huang, Q.; Leng, G.; Hou, B.; Ma, L. The propagation from meteorological to hydrological drought and its potential influence factors. *J. Hydrol.* **2017**, *547*, 184–195. [CrossRef]
7. Mishra, A.K.; Singh, V.P. A review of drought concepts. *J. Hydrol.* **2010**, *391*, 202–216. [CrossRef]
8. Liu, Y.; Zhu, Y.; Ren, L.; Singh, V.P.; Yong, B.; Jiang, S.; Yuan, F.; Yang, X. Understanding the spatiotemporal links between meteorological and hydrological droughts from a three-dimensional perspective. *J. Geophys. Res. Atmos.* **2019**, *124*, 3090–3109. [CrossRef]
9. Rousta, I.; Doostkamian, M.; Olafsson, H.; Ghafarian Malamiri, H.R.; Zhang, H.; Taherian, A.M.; Sarif, M.; Gupta, R.; MonroyVargas, E.R. On the relationship between the 500 hPa height fluctuations and the atmosphere thickness over Iran and the Middle East. *J. Mediterr. Meteorol. Climatol.* **2019**, *16*, 3–4. [CrossRef]
10. Guo, X.; Wang, T.; Li, Z.; Cheng, S.; Li, P.; Li, H.; Zhang, N.; Liu, X.; Miao, Z. Using PLE-SEM to Quantify the Impacts of Natural and Human Factors on Vegetation Change: A Case Study of the Jialing River Basin. *Sustainability* **2023**, *15*, 13089. [CrossRef]
11. Seneviratne, S.I.; Lüthi, D.; Litschi, M.; Schär, C. Land–atmosphere coupling and climate change in Europe. *Nature* **2006**, *443*, 205–209. [CrossRef] [PubMed]
12. Berg, A.; Lintner, B.R.; Findell, K.; Seneviratne, S.I.; VanDenHurk, B.; Ducharne, A.; Chéruy, F.; Hagemann, S.; Lawrence, D.M.; Malyshev, S.; et al. Interannual coupling between summertime surface temperature and precipitation over land: Processes and implications for climate change. *J. Clim.* **2015**, *28*, 1308–1328. [CrossRef]

13. Zampieri, M.; Toreti, A.; Ceglar, A.; Naumann, G.; Turco, M.; Tebaldi, C. Climate resilience of the top ten wheat producers in the Mediterranean and the Middle East. *Reg. Environ. Change* **2020**, *20*, 41. [CrossRef]
14. Vinzi, V.E.; Trinchera, L.; Amato, S. PLS path modeling: From foundations to recent developments and open issues for model assessment and improvement. In *Handbook of Partial Least Squares: Concepts, Methods and Applications*; Springer Nature: Berlin/Heidelberg, Germany, 2010; pp. 47–82.
15. Li, X.; Tian, Y.; Yang, M.; Wang, S. Cumulative effects of meteorological factors on low-flow change in the upper Yellow River. *Theor. Appl. Climatol.* **2024**, *155*, 8717–8730. [CrossRef]
16. Hayes, A.F.; Montoya, A.K.; Rockwood, N.J. The analysis of mechanisms and their contingencies: PROCESS versus structural equation modeling. *Australas. Mark. J.* **2017**, *25*, 76–81. [CrossRef]
17. Nogueira, J.M.; Rambal, S.; Barbosa, J.P.R.; Mouillot, F. Spatial pattern of the seasonal drought/burned area relationship across Brazilian biomes: Sensitivity to drought metrics and global remote-sensing fire products. *Climate* **2017**, *5*, 42. [CrossRef]
18. Marín, P.G.; Julio, C.J.; Arturo, R.-T.D.; Jose, V.-N.D. Drought and spatiotemporal variability of forest fires across Mexico. *Chin. Geogr. Sci.* **2018**, *28*, 25–37. [CrossRef]
19. Cepeda-Carrion, G.; Cegarra-Navarro, J.G.; Cillo, V. Tips to use partial least squares structural equation modelling (PLS-SEM) in knowledge management. *J. Knowl. Manag.* **2019**, *23*, 67–89. [CrossRef]
20. Wu, Z.; Lin, Q.; Lu, G.; He, H.; Qu, J.J. Analysis of hydrological drought frequency for the Xijiang River Basin in South China using observed streamflow data. *Nat. Hazards* **2015**, *77*, 1655–1677. [CrossRef]
21. Lin, Q.; Wu, Z.; Singh, V.P.; Sadeghi, S.H.R.; He, H.; Lu, G. Correlation between hydrological drought, climatic factors, reservoir operation, and vegetation cover in the Xijiang Basin, South China. *J. Hydrol.* **2017**, *549*, 512–524. [CrossRef]
22. Nie, C.; Li, H.; Yang, L.; Ye, B.; Dai, E.; Wu, S.; Liu, Y.; Liao, Y. Spatial and temporal changes in extreme temperature and extreme precipitation in Guangxi. *Quat. Int.* **2012**, *263*, 162–171. [CrossRef]
23. Lu, X.; Hideo, H.; Kiyoshi, T.; Yuzuru, M. Potential evapotranspiration methods for the assessment of river runoff under climate change. *Environ. Syst. Res.* **1998**, *26*, 357–362. [CrossRef]
24. Zhou, C.; Pan, B.; Jin, X. General situation and hydrologic characteristics of xijiang river basin. *Earth Environ. Sci.* **2020**, *514*, 022063. [CrossRef]
25. Fischer, T.; Gemmer, M.; Su, B.; Scholten, T. Hydrological long-term dry and wet periods in the Xijiang River basin. South China. *Hydrol. Earth Syst. Sci.* **2013**, *17*, 135–148. [CrossRef]
26. Ministry of Water Resources of the People's Republic of China. *Regulation for Hydrologic Computation of Water Resources and Hydropower Projects (SL278-2002)*; China Water & Power Press: Beijing, China, 2016.
27. McKee, T.B.; Doesken, N.J.; Kleist, J. The relationship of drought frequency and duration to time scales. In *Proceedings of the 8th Conference on Applied Climatology*; American Meteorological Society: Boston, MA, USA, 1993; Volume 17–22, pp. 179–183.
28. Yang, M.; Tian, Y.; Li, X.; Wei, Y.; Gan, F.; Yang, Y.; Wang, S. A novel coupled algorithm-based method, and the characteristics and driving mechanism of water shortage in the upper Yellow River. *Hydrol. Sci. J.* **2024**, *69*, 226–240. [CrossRef]
29. Thom, H.C. A note on the gamma distribution. *Mon. Weather. Rev.* **1958**, *86*, 117–122. [CrossRef]
30. Abramowitz, M.; Stegun, I.A. *Handbook of Mathematical Functions with Formulas, Graphs, and Mathematical Tables*; Dover Publications: New York, NY, USA, 1965.
31. Shah, R.; Bharadiya, N.; Manekar, V. Drought index computation using standardized precipitation index (SPI) method for Surat District, Gujarat. *Aquat. Procedia* **2015**, *4*, 1243–1249. [CrossRef]
32. Yang, X. Multi-Scale Spatiotemporal Distribution and Correlation Characteristics of Meteorological and Hydrological Droughts in the Yujiang River Basin Based on the SR and Copula Coupling. Master's Thesis, Guangxi University, Nanning, China, 2025.
33. Tenenhaus, M. Component-based structural equation modelling. *Total Qual. Manag.* **2008**, *19*, 871–886. [CrossRef]
34. Grace, J.B.; Schoolmaster, D.R., Jr.; Guntenspergen, G.R.; Little, A.M.; Mitchell, B.R.; Miller, K.M.; Schweiger, E.W. Guidelines for a graph-theoretic implementation of structural equation modeling. *Ecosphere* **2012**, *3*, 1–44. [CrossRef]
35. Lohmoller, J.B. The PLS program system: Latent variables path analysis with partial least squares estimation. *Multivar. Behav. Res.* **1988**, *23*, 125–127. [CrossRef]
36. Lin, Q.; Wu, Z.; Liu, J.; Singh, V.P.; Zuo, Z. Hydrological drought dynamics and its teleconnections with large-scale climate indices in the Xijiang River basin, South China. *Theor. Appl. Climatol.* **2022**, *150*, 229–249. [CrossRef]
37. Lin, Q.; Wu, Z.; Zhang, Y.; Peng, T.; Chang, W.; Guo, J. Propagation from meteorological to hydrological drought and its application to drought prediction in the Xijiang River basin, South China. *J. Hydrol.* **2023**, *617*, 128889. [CrossRef]
38. Ding, Y.; Lu, Z.; Wu, L.; Zhou, L.; Ao, T.; Xu, J.; Wei, R. Evaluating the spatiotemporal dynamics of driving factors for multiple drought types in different climate regions of China. *J. Hydrol.* **2024**, *640*, 131710. [CrossRef]
39. Ding, Y.; Zhang, L.; He, Y.; Cao, S.; Wei, X.; Guo, Y.; Filonchyk, M. Spatiotemporal evolution of agricultural drought and its attribution under different climate zones and vegetation types in the Yellow River Basin of China. *Sci. Total Environ.* **2024**, *914*, 169687. [CrossRef]

40. Zhu, Q.; Zhang, H. Groundwater drought characteristics and its influencing factors with corresponding quantitative contribution over the two largest catchments in China. *J. Hydrol.* **2022**, *609*, 127759. [CrossRef]
41. Jin, H.; Zhang, K.; Zhang, P.; Liu, G.; Liu, M.; Chen, X.; Willems, P. Spatiotemporal evolution of drought status and its driving factors attribution in China. *Sci. Total Environ.* **2025**, *958*, 178131. [CrossRef]
42. Yu, S.; Wang, L.; Zhao, J.; Shi, Z. Using structural equation modelling to identify regional socio-economic driving forces of soil erosion: A case study of Jiangxi Province, southern China. *J. Environ. Manag.* **2021**, *279*, 111616. [CrossRef]
43. Wu, Y.; Bake, B.; Zhang, J.; Rasulov, H. Spatio-temporal patterns of drought in North Xinjiang, China, 1961–2012 based on meteorological drought index. *J. Arid. Land* **2015**, *7*, 527–543. [CrossRef]
44. Yang, Y.; Xie, N.; Gao, M. The relationship between the wintertime cold extremes over East Asia with large-scale atmospheric and oceanic teleconnections. *Atmosphere* **2019**, *10*, 813. [CrossRef]
45. Yang, P.; Xia, J.; Zhang, Y.; Han, J.; Wu, X. Quantile regression and clustering analysis of standardized precipitation index in the Tarim River Basin, Xinjiang, China. *Theor. Appl. Climatol.* **2018**, *134*, 901–912. [CrossRef]
46. Yang, R.; Xing, B. Teleconnections of large-scale climate patterns to regional drought in mid-latitudes: A case study in Xinjiang, China. *Atmosphere* **2022**, *13*, 230. [CrossRef]
47. Rousta, I.; Olafsson, H.; Moniruzzaman, M.; Zhang, H.; Liou, Y.A.; Mushore, T.D.; Gupta, A. Impacts of drought on vegetation assessed by vegetation indices and meteorological factors in Afghanistan. *Remote Sens.* **2020**, *12*, 2433. [CrossRef]
48. Zaitchik, B.F.; Macalady, A.K.; Bonneau, L.R.; Smith, R.B. Europe's 2003 heat wave: A satellite view of impacts and land–atmosphere feedbacks. *Int. J. Climatol.* **2006**, *26*, 743–769. [CrossRef]
49. Saft, M.; Western, A.W.; Zhang, L.; Peel, M.C.; Potter, N.J. The influence of multiyear drought on the annual rainfall-runoff relationship: An a ustralian perspective. *Water Resour. Res.* **2015**, *51*, 2444–2463. [CrossRef]
50. Craig, R.K. Stationarity is dead-long live transformation: Five principles for climate change adaptation law. *Harv. Environ. Law Rev.* **2010**, *34*, 9.
51. Chiew, F.H.; Peel, M.C.; McMahon, T.A.; Siriwardena, L.W. Precipitation elasticity of streamflow in catchments across the world. *IAHS Publ.* **2006**, *308*, 256.
52. Petheram, C.; Potter, N.; Vaze, J.; Chiew, F.; Zhang, L. Towards better understanding of changes in rainfall-runoff relationships during the recent drought in south-eastern Australia. In Proceedings of the 19th International Congress on Modelling and Simulation, Perth, Australia, 12–16 December 2011; pp. 12–16.
53. Chiew, F.H.S.; Potter, N.J.; Vaze, J.; Petheram, C.; Zhang, L.; Teng, J.; Post, D.A. Observed hydrologic non-stationarity in far south-eastern Australia: Implications for modelling and prediction. *Stoch. Environ. Res. Risk Assess.* **2014**, *28*, 3–15. [CrossRef]
54. Potter, N.J.; Petheram, C.; Zhang, L. Sensitivity of streamflow to rainfall and temperature in south-eastern Australia during the Millennium drought. In Proceedings of the 19th International Congress on Modelling and Simulation, Perth, Australia, 12–16 December 2011; pp. 3636–3642.
55. Tian, W.; Liu, X.; Liu, C.; Bai, P. Investigation and simulations of changes in the relationship of precipitation-runoff in drought years. *J. Hydrol.* **2018**, *565*, 95–105. [CrossRef]
56. Jia, Z.; Lin, T.; Guo, X.; Zheng, Y.; Geng, H.; Zhang, J.; Chen, Y.; Liu, W.; Lin, M. Vegetation greening mitigates the positive impacts of climate change on water availability in Northwest China. *J. Hydrol.* **2024**, *644*, 132086. [CrossRef]
57. Ye, Q.; Li, Z.; Duan, L.; Xu, X. Decoupling the influence of vegetation and climate on intra-annual variability in runoff in karst watersheds. *Sci. Total Environ.* **2022**, *824*, 153874. [CrossRef]

https://doi.org/10.3390/hydrology13050131